

RELEVANCE OF COLD-ROLLING TECHNOLOGY FOR THE TEXTURE AND ANISOTROPY OF EN AW-8011A ALUMINUM ALLOYS

USTREZNOST TEHNOLOGIJE HLADNEGA VALJANJA ZA TEKSTURO IN ANIZOTROPIJO ALUMINIJEVE ZLITINE EN AW-8011A

Jakob Kraner^{1*}, Kyung Il Kim², Bonghwan Kim², Shae K. Kim², Irena Paulin³

¹Impol Aluminium Industry, Partizanska 38, 2310 Slovenska Bistrica, Slovenia

²Korea Institute of Industrial Technology, KITECH, 21999 Incheon, Republic of Korea

³Institute of Metals and Technology, IMT, Lepi pot 11, 1000 Ljubljana, Slovenia

Prejem rokopisa – received: 2023-09-10; sprejem za objavo – accepted for publication: 2023-10-10

doi:10.17222/mit.2023.993

The combined effects of the reduction ratio and annealing conditions during cold rolling were investigated for the texture and anisotropy of an EN AW-8011A aluminium alloy. To characterize the microstructural and textural differences, a scanning electron microscope with electron back-scattered diffraction was used. To achieve low anisotropy, the three key factors of texture were exposed: a low fraction of deformed grains according to the average grain misorientation, a large amount of random texture components and the equivalent ratio between deformed and recrystallised texture components. The results of crystallographic texture analysis and anisotropy values revealed that the higher ratio of total cold deformation (cold rolling reduction) and the higher ratio of cold deformation after the intermediate annealing were more favourable for the final continuous annealing in terms of decreasing anisotropy. In contrast, the lower ratio of the cold deformation resulted in lower anisotropy when implementing batch annealing.

Keywords: aluminium alloys, cold rolling, SEM-EBSD, textures, anisotropy

Vplivi ob spreminjanju stopnje redukcije in pogojev medfaznega žarjenja med hladnim valjanjem so bili raziskovani na podlagi kristalografskih tekstur in anizotropije za aluminijevo zlitino EN AW-8011A. Vrščni elektronski mikroskop s tehniko uklona povratno sipanih elektronov je bil uporabljen za karakterizacijo mikrostrukturnih in teksturnih razlik. Nadalje so za doseganje nizke anizotropije bili izpostavljeni: majhen delež deformiranih zrn po kriteriju povprečne dezorientacije zrn, visok delež naključno orientiranih teksturnih komponent in enakovredno razmerje med deformacijskimi in rekristalizacijskimi teksturnimi komponentami, kot trije ključni faktorji, ki so povezani s kristalografsko teksturo materiala. Rezultati teksturnih analiz in vrednosti pokazateljev anizotropije so razkrili, da sta večja skupna hladna deformacija (večja skupna redukcija) in večja hladna deformacija po medfaznem žarjenju ugodnejši za kontinuirno končno žarjenje in manj primerni za serijsko-komorno žarjenje. V nasprotju sta tanjša debelina vroče valjanega traku in manjša skupna hladna deformacija po medfaznem žarjenju povzročili manjšo anizotropijo materiala po serijskem-komornem kot v primeru kontinuirnega končnega žarjenja.

Ključne besede: aluminijeve zlitine, hladno valjanje, SEM-EBSD, teksture, anizotropija

1 INTRODUCTION

Cold rolling is one of the most common metal-forming processes. In the metallurgical production step of flat-rolled products, cold rolling is carried out after direct chill (DC) casting and hot rolling.¹ Recrystallised or partially recrystallised, hot-rolled microstructures obtained by hot rolling are transformed to the longitudinal and flattened crystal grains by subsequent cold rolling, deformation under recrystallisation temperature.² Higher deformation by cold rolling leads to finer crystal grains, but each aluminium alloy has the specific limitation of admissible total deformation before the break.³ Therefore, between cold-rolling passes, the intermediate annealing needs to be taken to relieve the stored energy (strains) and enable further cold rolling to the final foil thick-

nesses.⁴ According to the required mechanical properties and texture, the number and regime of the intermediate and final annealings are chosen. Besides mechanical properties, cold rolling affects the grain size, texture orientation and elongation, which are strongly connected to anisotropy.⁵

The cold rolling of aluminium alloys with a face-centred cubic (FCC) crystal structure generally creates a specific, fibre-oriented texture: α -fibre for the smaller deformations and β -fibre for the larger deformations.⁶ β -fibre represents the union of the three most common deformed (rolling) texture components.⁷ Intermediate annealing generally results in more recrystallised texture components. The deformed texture components exhibit anisotropy that is opposite to the recrystallised texture components.⁸ The anisotropy analysis of deformed material shows ears in the case of deep-drawn aluminium cups at an angle of 45° to the rolling direction. In contrast, the ears of the annealed material occur in the roll-

*Corresponding author's e-mail:
jakob.kraner@impol.si (Jakob Kraner)

Table 1: Chemical compositions of foils (0.09 mm) in wt.% (the measurements error is ± 0.02)

	Si	Fe	Mn	Mg	Cu	Ti	Al
STANDARD EN AW-8011A	0.65-0.80	0.65-0.75	0.08-0.10	0.03-0.05	<0.1	0.02-0.04	Bal.
Technology A	0.70	0.70	0.087	0.033	0.01	0.028	Bal.
Technology B	0.72	0.72	0.089	0.034	0.01	0.026	Bal.

Table 2: Cold-rolling technologies

	Technology A	Technology B
Thickness of as-hot rolled (RFS)	6 mm ± 0.05 mm	3.25 mm ± 0.05 mm
Thickness of 1 st as-cold rolled / reduction ratio (1C)	1.5 mm ± 0.05 mm / 75 %	0.9 mm ± 0.05 mm / 75 %
Parameters of intermediate annealing (IA)	400 °C ± 10 °C, 4 h	400 °C ± 10 °C, 4 h
Thickness of 2 nd as-cold rolled / reduction ratio (2C)	0.09 mm ± 0.05 mm / 95 %	0.09 mm ± 0.05 mm / 85 %
Parameters of final batch or continuous annealing (FBA or FCA)	270 °C ± 5 °C and 320 °C ± 5 °C Batch 1 h, Continuous 2–4 min	

ing direction (0°) and perpendicular to the rolling direction (90°).^{9,10} To achieve the maximum achievable isotropy (low earing of a cup), a constructive ratio between deformed and recrystallised texture components is required.

Selecting the most common texture components for the analysis often does not embrace the whole textures share. S. Li et al.¹¹ introduced the random texture components, which are defined as the percentage difference in the total share of textures. Due to the variety of texture components in the random texture components, a significant fraction of them has a beneficial influence on reducing anisotropy. This is based on the calculation of J. Sidor et al.,¹² which predicted anisotropy values for each texture component according to the Miller indices. The predicted anisotropy values are negative for the deformed texture components, while positive for the recrystallised texture components. The description proposes the benefit of a higher proportion of random texture components and the desired ratio between deformed and recrystallised texture components. The smallest possible difference between positive and negative predicted anisotropy values will lead to the lower earing of cup, as stated by W. Liu et al.¹³

The importance of two crystallographic texture-related factors can be upgraded by introducing one new independent impact on the anisotropy. According to the grains' average misorientation (GAM) theory, crystal grains can be divided into the groups of deformed, substructured and recrystallized.¹⁴ GAM analysis cannot be directly implemented to calculate anisotropy, which relies on the random texture components and the deformed and recrystallised texture components ratio, but can represent the general achievement factor for the material of low anisotropy. An excessive proportion of GAM criteria determined in deformed grains will result in elevated levels of anisotropy, even in cases where there is a greater presence of random texture components and an optimal ratio between the deformed and recrystallized texture components ($DEF_{\text{textures}} / REX_{\text{textures}} = 1.0$).

This article presents a systematic tracking of the crystallographic texture evolution for the aluminium al-

loy EN AW-8011A during cold rolling. Electron back-scatter diffraction (EBSD) maps obtained with a scanning electron microscope (SEM) are evaluated in detail to obtain quantitative data about the presence of individual textural components. The main purpose is to introduce three factors in conjunction with the deformed FCC grains according to the GAM criteria: the proportion of random-orientated texture components and the ratio between the deformed and recrystallised texture components to ensure low anisotropy values. The first factor is the important basis for low anisotropy since the excessively high share of deformed grains is insufficient to ensure low ears of the extracted cups. The other two factors can be used to calculate the anisotropy value from the proportions of texture components, which are proportionally orientated with the measured values of ears on the extracted cups.

2 MATERIALS AND METHODS

The materials in the current study are cold-rolled sheets and foils of aluminium alloy EN AW-8011A. The chemical composition was determined with the ICP-OES technique and is presented in **Table 1**. The hot-rolled band was industrially rolled to thicknesses of 6.00 mm and 3.25 mm. The two initial materials are marked as re-roll foil stock (RFS). Further industrial cold rolling was made with the same pattern for both thicknesses of RFS. The 6-mm rolling technology (Technology A) and the 3.25-mm rolling technology (Technology B) consisted of cold rolling to a total deformation of 75 % (1C). It continued with the intermediate annealing at 400 °C for 4 h (IA). Annealed coils were cold rolled to a final thickness of 0.09 mm (2C). For the final thickness, the final annealing was performed by batch (FBA) or continuous (FCA) techniques. The FBA was performed between 270 °C and 320 °C for 1 h, when the material in the furnace reached the set temperature. The compared FCA was performed at the same temperatures (270 °C and 320 °C) for only between 2 min and 4 min (**Table 2**).

The samples for the microstructural studies were sectioned parallel to the rolling direction. For the

SEM-EBSD analyses the samples were mechanically ground with SiC papers and polished with diamond slurries. A ZEISS CrossBeam 550 equipped with an EBSD detector (EDAX Hikari Super plus camera) was used for the microstructural and crystallographic studies. Step sizes of 0.5 μm were used to scan the mappings. The magnification was proportionally increased with the thickness reduction of rolled aluminium samples (200×–500×). OIM Analysis software was used for the inverse pole figures (IPF-Z), the GAM images and the texture components' data acquisition. The considered GAM criteria were 0°–0.5° of misorientation for the recrystallised grains, 0.5°–2° for the substructured grains and 2°–5° for the deformed grains. The detailed analyses of texture components contained the four most common deformed and four most common recrystallised texture components (Table 3).

Table 3: Eight selected most common texture components in FCC material with their Miller indices and predicted anisotropy values Δr¹²

Texture type	Designation of texture component	Miller indices		Predicted anisotropy Δr
		{hkl}	<uvw>	
Deformed texture components	C	{1 1 2}	<1 1 1>	–5.7
	S	{1 2 3}	<6 3 4>	–5.1
	B	{0 1 1}	<2 1 1>	–8.1
	D	{4 4 11}	<11 11 8>	–3.3
Recrystallised texture components	Cube	{0 0 1}	<1 0 0>	1.0
	G	{1 1 0}	<0 0 1>	30.0
	R	{1 2 4}	<2 1 1>	1.2
	P	{0 1 1}	<1 1 2>	1.6

The values of the predicted anisotropy Δr for the analyses including texture components are in accordance with their Miller indices, as published by J. Sidor et al.¹² For the calculation of anisotropy from EBSD measurements (Δr_{texture}) each fraction (marked with X, where i = C, S, B, D, Cube, G, R and P) of individual texture component was multiplied with their corresponding Δr as presented in equation (1):

$$\Delta r_{\text{texture}} = X_C \cdot \Delta r_C + X_S \cdot \Delta r_S + X_B \cdot \Delta r_B + X_D \cdot \Delta r_D + X_{\text{Cube}} \cdot \Delta r_{\text{Cube}} + X_G \cdot \Delta r_G + X_R \cdot \Delta r_R + X_P \cdot \Delta r_P \quad (1)$$

The improved and more accurate calculated anisotropy of material Δr_{material} from the EBSD measurements must contain the value of the random texture components X_{Random}, which has a positive effect on reducing the anisotropy with the increasing X_{Random} fraction. The Δr_{material} can be calculated with equation (2):

$$\Delta r_{\text{material}} = \frac{(100 - x_{\text{Random}}) \cdot \Delta r_{\text{texture}}}{100} \quad (2)$$

The mechanical properties were measured according to ISO 6892-1:2016 (tensile test in rolling direction RD). For the acquisition of ultimate tensile strength R_m, the yield strength R_{p0.2} and the elongation A results the Zwick Roell Z050 testing machine was used. The earing

cup test – anisotropy was performed in accordance with the ISO 11531:2015 standard. For the extraction of the cups, an Erichsen 134 machine was used and further the ears on the cups were evaluated with a Erichsen 126 PLUS measuring tool. All the mechanical properties and anisotropy results are presented as an average of 5 representative measurements.

3 RESULTS AND DISCUSSION

In Figure 1a the microstructural development with the SEM-EBSD micrographs (IPF-Z) of Technology A is presented. The grains transformation before and after IA, FBA or FCA is clearly shown. The most outstanding difference is observed when comparing the grain sizes of FBA and FCA. For the latter the grains are significantly finer. Further, in Figure 1b the same micrographs are processed in accordance with the GAM criteria (using directly on the same SEM-EBSD mappings for more accurate result presentation). The compared different final annealed samples do not differ so distinctly according to the GAM criteria. The final annealed samples are similar to the initial RFS 6-mm material for the mentioned criteria.

The same micrograph presentation as for Technology A with the SEM-EBSD mappings (IPF-Z) in Figure 2a and GAM criteria in Figure 2b are formed also for Technology B. Comparing both RFS samples, the smaller grains are present at the initial RFS 3.25 mm. Furthermore, a larger fraction of deformed grains (according to GAM) is observed for the thinner RFS. Nevertheless, the IPF-Z micrographs of the IA samples of the compared technologies are similar to the GAM-analysed micrographs, revealing the key differences. More deformed grains are present in the final microstructure of an IA sample, which belongs to Technology B. Observing the grain size, shape and orientation in IPF-Z and GAM micrographs, there is no major difference between FBA or FCA comparing Technology A and Technology B.

The larger produced fraction of deformed grains with a lower thickness of RFS is after the same cold deformation as a consequence, present also after the IA. Stated is also emphasised with the higher fraction of substructured grains, which are closer to the shape and misorientation of the deformed than the recrystallised grains. As described, the microstructural influence of RFS is transferred further in the process steps, which requires additional attention when performing the heat treatment.^{15,16} According to the GAM analysis, higher temperature or longer time must be applied for IA so that the share of deformed grains in the Technology B micrograph will approach the Technology A micrograph.¹⁷ However, the proposed change is not absolutely necessary to achieve the desired final mechanical, microstructural and formability properties.¹⁸

The development of crystallographic textures during the process of cold rolling with Technology A is pre-

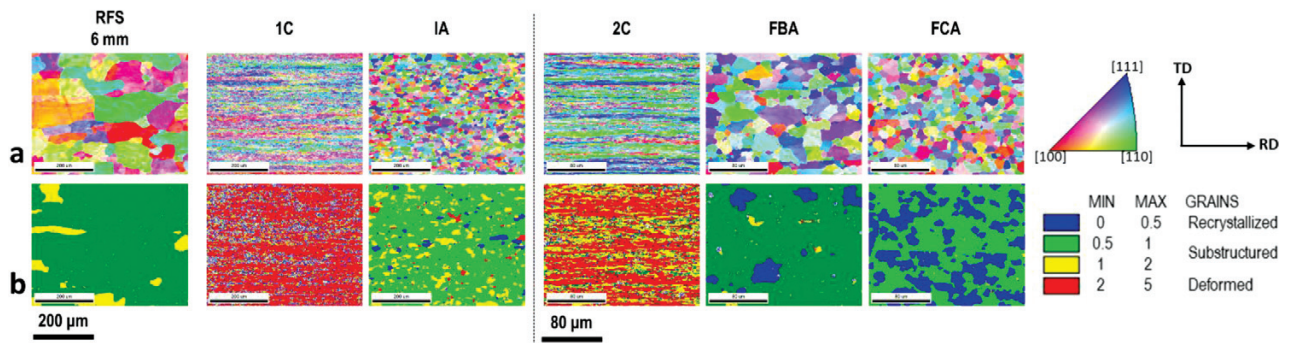


Figure 1: Microstructure development by Technology A: a) inverse pole figures in Z direction (IPF-Z), b) grain average misorientation (GAM)

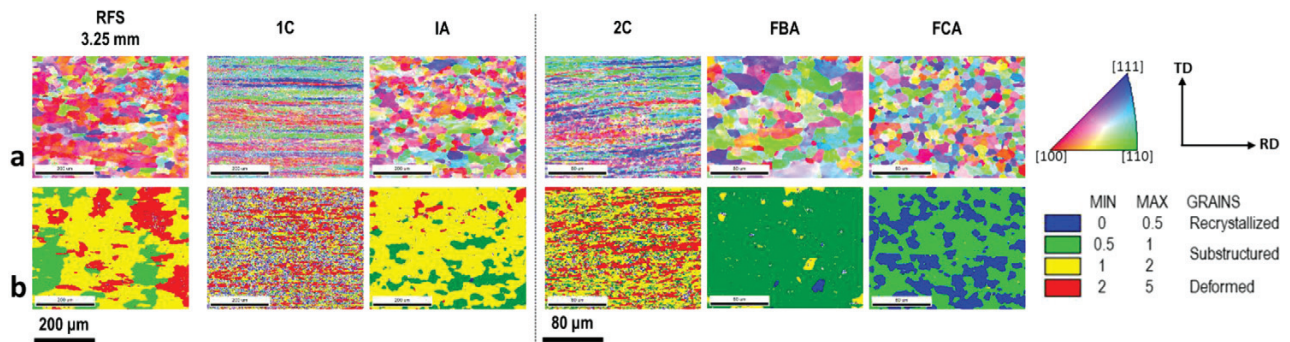


Figure 2: Microstructure development by Technology B: a) inverse pole figures in Z direction (IPF-Z), b) grain average misorientation (GAM)

sented in **Figure 3a**. There are more deformed and recrystallised texture components with a percentage higher than 15 %. The two times outstanding percentage for texture component P is higher than 26 %. Comparing the before and after annealed states of material shares of deformed and recrystallised texture components alternate coincidental. The clearest examples of the described texture variations are observed for texture component B, where for samples 1C and 2C, the fractions increase to 17 % and 21 %. In contrast, the a significant increase of texture component R share in comparison to the deformed states is increased after IA and both FBA and FCA. A similar path is also observed for texture compo-

nents P, except for material 1C, where the share is extremely high and is surpassed only in the case of FBA.

In **Figure 3b** the texture components' fraction during the cold-rolling process with Technology B are presented. The highest fractions of deformed and recrystallised texture components are under 20 %. Unlike the Technology A materials after IA, FBA and FCA have a significant share of the cube texture component. The texture component has a high fraction of 19 %, also in the case of RFS. The dominant recrystallisation texture component for RFS in the case of Technology A is R. Similar to the compared cold rolling 1C and 2C material the

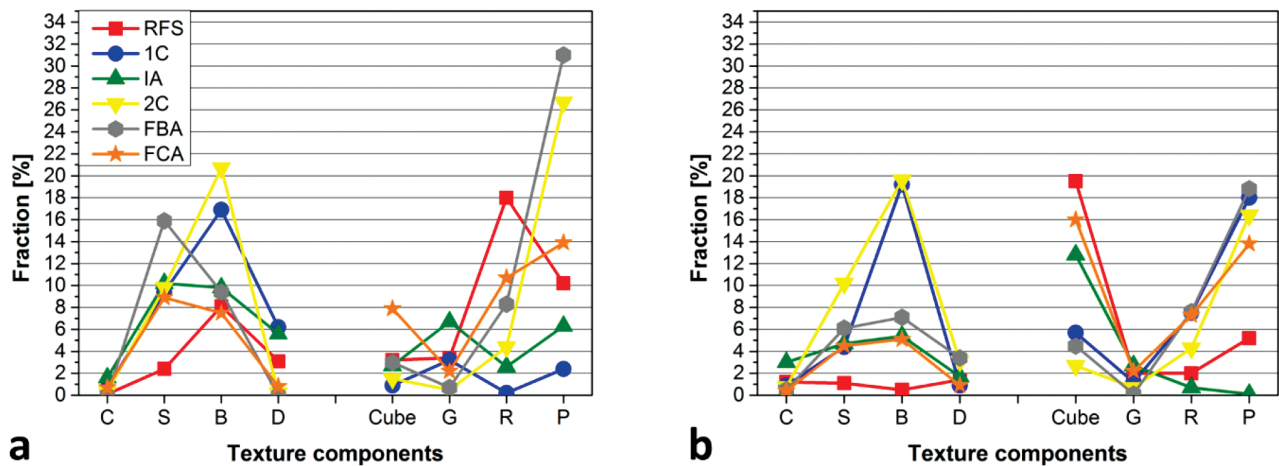


Figure 3: Fraction of texture components: a) technology A, b) technology B

share of texture component B is increased to the values around 20 %.

Thicker RFS material has higher fraction values of deformed texture components than thinner RFS, where all the fractions of the deformed texture components are less than 2 %. After the IA of thicker RFS, the fraction of all four recrystallised texture components is approximately increased compared to the 1C material. The described path of the recrystallised texture components enlargement after IA is completed just in case of the cube and G texture components. The fraction of texture components R and P is lower after (IA) than before (1C), but the predominant 13 % of cube texture components can have a key influence on the isotropy's establishment.^{19,20} Both compared textures in 2C material have one predominant deformed (B) and one predominant recrystallised (P) texture component, which is theoretically good for achieving a low anisotropy.²¹ After the FBA, the high

fraction of the P texture component is not annulled in both cases of rolling technologies. But it is a predominant share of B texture component reduced below 10 % in both cases. The FBA, in the case of Technology A, provides the exchange of dominant deformed texture components from B to S, which has a less negative influence on the predicted anisotropy.^{6,12} The fraction of all four observed deformed texture components after FCA is lower in the case of Technology B than in Technology A. Despite that, the fraction of observed recrystallised texture components after the mentioned final annealing is similar for the compared rolling technologies. The details can have an influence on the results of the anisotropy. A higher fraction of the cube texture component, which transfers throughout the cold rolling process of Technology B, can be the reason for higher anisotropy values of FCA foil.²²

A detailed analysis led to the exposure of three important parameters for providing low material anisotropy. **Figure 4a** presents the variation of deformed grains fraction (GAM) during the cold-rolling and annealing processes. As expected for Technology A, drastic increases of deformed grains are observed for samples 1C and 2C. For the case of Technology B, the deformed grains are present already at RFS, but the increase of the deformed grains' fraction with the cold rolling is barely noticeable. The fraction of deformed grains before (1C) intermediate or final (2C) annealing is much more equal for Technol-

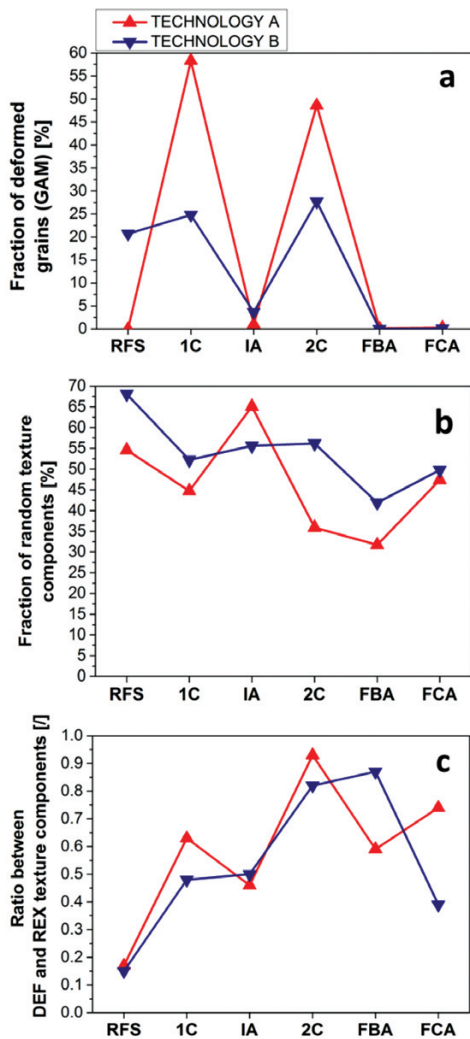


Figure 4: Exposed parameters, which have a major influence on the successful achieving of low anisotropy values: a) fraction of deformed grains according to GAM criteria, b) fraction of random texture components, c) ratio between deformed and recrystallised texture components

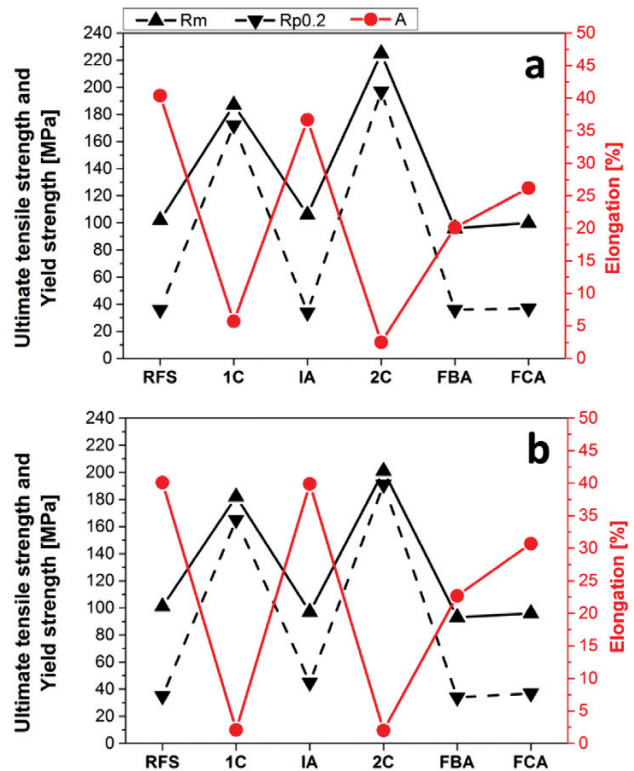


Figure 5: Changes in the mechanical properties during cold rolling: a) technology A, b) technology B (defined measurements error for Rm and Rp_{0.2} is ±5 MPa and for A is ±2 %)

ogy B, than in the case of Technology A, where the 10 % difference was observed. Regardless of the implemented rolling technology, the fraction of deformed grains after IA, FBA, and FCA was always less than 2 %. In **Figure 4b**, the variation of random texture components fractions for the compared cold-rolling technologies is presented. The lowest values of random texture components for both cold rolling technologies are observed for the FBA samples. In the case of Technology B, the highest fraction of random texture components is at RFS, for the Technology A sample after IA shows the highest randomization of the texture components. Both compared samples after FCA have the most similar values throughout the entire compared technological chains. The statement clearly explains the crucial difference between FBA and FCA in achieving low anisotropy values based on random texture components present in the material. **Figure 4c** shows changing the ratio between deformed and recrystallised texture components compared to Technology A and Technology B. After the initial low ratio (0.15) for both compared cold-rolling technologies, the calculated ratio for Technology A increased before intermediate (1C) and final (2C) annealing, and it is always decreased after annealing. For Technology B, the ratio between the deformed and recrystallised texture components is constantly increased with the process steps, where the trend is continued with the FBA and reversed in the case of FCA because the calculated ratio is decreased. For the criteria of the ratio between deformed and recrystallised texture components, the difference between the compared cold-rolling technologies is most obvious. The less deformation after IA (Technology B, blue curve) resulted in more suitable ratio for lower anisotropy after FBA than FCA as for technology B (blue line) a lower ratio (increased recrystallization fractions) is at FCA compared to FBA). In contrast, the higher cold deformation after IA (Technology A) provides a better ratio for lower anisotropy after FCA than FBA.

The presented mechanical properties in **Figure 5a** for Technology A and in **Figure 5b** for Technology B are similar during both cold-rolling processes. The *R_m* values are independent of the cold rolling technology for RFS after (IA) and final (FBA or FCA) annealing, al-

ways around 100 MPa. The major difference is observed for 2C samples with 30-MPa higher values of *R_m* in the thicker RFS than the thinner RFS cold rolling technology. This is a consequence of a higher percentage of deformation after IA using Technology A. The importance of the material's thickness for IA is also recognised for *A* values after FBA or FCA. In both cases of cold rolling technologies, the *A* is higher after FCA, which fully coincides with the smaller crystal grains compared to the FBA microstructure. The *A* values after both types of final annealing (FBA or FCA) for Technology B are, in general, higher by 2 % to 5 %, which can be attributed to a smaller total deformation after the IA.

In **Table 4**, the results of anisotropy indicators are presented. For Technology A the *E_a* values increase from RFS (1.03 %) to the cold rolled 2C material (6.55 %) with the double change of ears angle on the cups according to the rolling direction. The mentioned double change of ears angle is also observed compared to Technology B. In contrast to the compared cold rolling technology the *E_a* value after IA is decreased from 2.20 % to 1.52 %, which is similar to the value as at RFS (1.79 %). The lowest *E_a* value after FCA (0.70 %) is reached with Technology A, which can be characterised as the most successful cold-rolling technology. Using FBA, Technology B is a better option based on the lower *E_a* value (1.09 %). According to the reached *E_a* values, Technology B can be with greater reliability used for both FBA and FCA techniques.

The calculated $\Delta r_{\text{material}}$ are excellent support for *E_a* and *E_a*_{angle} values because they correctly predicted the values despite the cold rolling technology or material state. The *E_a*_{angle} is announced with negative $\Delta r_{\text{material}}$ for ears orientation 45° according to the rolling direction and positive $\Delta r_{\text{material}}$ for ears orientated 90° according to the rolling direction. Furthermore, the $\Delta r_{\text{material}}$ values in intervals (0–20, 20–40, 40–60, etc.) match with the groups of *E_a* results (0–1 %, 1–2 %, 2–3 %, etc.). The described results connections enable the approximate prediction of material's anisotropy with the SEM-EBSD data.¹²

Table 4: Anisotropy results comparison for different cold-rolling technologies according to the measured ears on the extracted cup (*E_a*) with the angle of ears appearance (*E_a*_{angle}) and calculated values $\Delta r_{\text{material}}$ from the SEM-EBSD data

	Technology A			Technology B		
	Earing on cups <i>E_a</i> (%)	Angle of ears on cups <i>E_a</i> _{angle} (°)	Calculation of anisotropy $\Delta r_{\text{material}}$ (I)	Earing on cups <i>E_a</i> (%)	Angle of ears on cups <i>E_a</i> _{angle} (°)	Calculation of anisotropy $\Delta r_{\text{material}}$ (I)
RFS	1.03	90	24.8	1.79	90	22.0
1C	1.94	45	-59.6	2.20	45	-50.9
IA	2.38	90	26.3	1.52	90	12.3
2C	6.55	45	-99.7	6.12	45	-74.7
FBA	2.45	45	-50.3	1.09	45	-32.5
FCA	0.7	45	-2.0	1.67	90	21.8

4 CONCLUSIONS

This work presents a systematic and comparative study of the influences of cold rolling, and intermediate and final annealing on the anisotropy of EN AW-8011 aluminium alloy. The focus was on the three factors of the deformed grains based on GAM, the random texture components and the ratio between deformed and recrystallised texture components. Furthermore, the predicted anisotropy was calculated to evaluate the connection between anisotropy and texture. The following conclusions can be drawn:

- Between the selected technological parameters, the total cold deformation before and after intermediate annealing has a crucial influence on achieving low anisotropy, especially if different initial thicknesses for cold rolling and the final annealing methods are used.
- According to the crystallographic texture analysis and anisotropy values, the thicker hot-rolled band and larger total cold deformation after the intermediate annealing are more favourable for the continuous final annealing. In contrast, the thinner hot-rolled band and the smaller total cold deformation results in lower anisotropy by batch annealing.
- The three factors for achieving the low anisotropy values are recognised as the low fraction of deformed grains according to the GAM criteria, the high amount of random texture components, and the ideal ratio between deformed and recrystallised texture components (value 1).
- In the cold rolling and annealing processes for the thicker band, a more pronounced variation in the fraction of random texture components was observed compared to the thinner band. The noteworthy distinctions, which align with anisotropy, can be attributed to the ratio between deformed and recrystallised texture components. It is worth noting that the only discernible difference between differently performed final annealing.
- The calculated anisotropy values based on the texture components and random texture shares match well with the measured ears on the extracted cups. Also, the positive or negative calculated values match with the ears location on the cups according to the rolling direction.

Acknowledgement

This work was carried out within the framework of the Slovenian Research and Innovation Agency ARRS L2-3164 and ARRS programme P2-0132.

5 REFERENCES

- ¹ J. Hirsch, Aluminium sheet fabrication and processing. *Fund. Alumin. Metal.*, (2011), 719–746, doi:10.1533/9780857090256.3.719
- ² J. Kraner, T. Smolar, D. Volšak, M. Lažeta, R. Skrbinek, D. Fridrih, P. Cvahte, M. Godec, I. Paulin, Influence of the hot-rolling technique for EN AW-8021B aluminium alloy on the microstructural properties of a cold-rolled foil, *Mater. Tehnol.*, 55 (2021), 773–779, doi:10.17222/mit.2021.216
- ³ Y. Wang, F. Yang, L. Ren, Q. Liu, Y. Cao, G. Huang, Microstructure and texture of an aluminium plate produced by multipass cold rolling and graded annealing process, *Metals*, 12 (2022), 260, doi:10.3390/met12020260
- ⁴ H. Takuda, N. Yamazaki, N. Hatta, S. Kikuchi, Influence of cold-rolling and annealing conditions on formability of aluminium alloy sheet, *J. Mater. Sci.*, 30 (1995), 957–963, doi:10.1007/BF01178430
- ⁵ M. Fourmeau, T. Børvik, A. Benallal, O. G. Lademo, O.S. Hopperstad, On the plastic anisotropy of an aluminium alloy and its influence on constrained multiaxial flow, *Int. J. Plastic*, 27 (2011), 2005–2025, doi:10.1016/j.ijplas.2011.05.017
- ⁶ J. Hirsch, T. Al-Samman, Superior light metals by texture engineering: Optimized aluminum and magnesium alloys for automotive applications, *Acta Mater.*, 61 (2013), 818–843, doi:10.1016/j.actamat.2012.10.044
- ⁷ J. Kraner, T. Smolar, D. Volšak, P. Cvahte, M. Godec, I. Paulin, A review of asymmetric rolling, *Mater. & Tech.*, 54 (2020) 731–743, doi:10.17222/mit.2020.158
- ⁸ N. Kishor, D. Ravi Kumar, Optimization of initial blank shape to minimize earing in deep drawing using finite element method, *J. Mater. Process. Tech.* 130-131 (2002), 20–30, doi:10.1016/S0924-0136(02)00790-2
- ⁹ O. Engler, J. Hirsch, Polycrystal-plasticity simulation of six and eight ears in deep-drawn aluminium cups, *Mater. Sci. & Eng. A*, 452-453 (2007), 640–651, doi:10.1016/j.msea.2006.10.108
- ¹⁰ S. Izadpanah, S. H. Ghaderi, M. Gerdooei, Prediction of earing in deep drawing of anisotropic aluminum alloy sheet using BBC2003 yield criterion, *J. Comp. & App. Resear. Mech. Eng.*, 6 (2017), 47–55, doi:10.22061/jcarme.2017.583
- ¹¹ S. Li, Q. Zhao, Z. Liu, F. Li, A review of texture evolution mechanisms during deformation by rolling in aluminium alloys, *J. Mater. Eng. & Perform.*, 27 (2018), 3350–3373, doi:10.1007/s11665-018-3439-y
- ¹² J. Sidor, A. Miroux, R. Petrov, L. Kestens, Microstructural and crystallographic aspects of conventional and asymmetric rolling processes, *Acta Mater.*, 56 (2008), 2495–2507, doi:10.1016/j.actamat.2008.01.042
- ¹³ W. Liu, J. Huang, Y. Pang, K. Zhu, S. Li, J. Ma, Multi-scale modelling of evolving plastic anisotropy during Al-alloy sheet forming, *Int. J. Mech. Sci.*, 247 (2023), doi:10.1016/j.ijmecs.2023.108168
- ¹⁴ C. Zheng, Y. Wang, J. Jin, P. Gong, X. Wang, H. Wen, M. Zhang, Recrystallization and grain growth behavior of variously deformed CoCrFeMnNi high-entropy alloys: microstructure characterization and modelling, *J. Mater. Resear. & Tech.*, 20 (2022) 2277–2292, doi:10.1016/j.jmrt.2022.07.182
- ¹⁵ R. K. Gupta, R. Panda, A.K. Mukhopadhyay, V. Anil Kumar, P. Sankaravelayutham, K. M. George, Study of Aluminum Alloy AA2219 After Heat Treatment, *Met. Sci. & Heat Treat.*, 57 (2015) 350–353, doi:10.1007/s11041-015-9888-0
- ¹⁶ B. Wang, X. Chen, F. Pan, J. Mao, Y. Fang, Effects of cold rolling and heat treatment on microstructure and mechanical properties of AA 5052 aluminum alloy, *Trans. Nonferrous Met. Soc. China*, 25 (2015) 2481–2489, doi:10.1016/S1003-6326(15)63866-3
- ¹⁷ J. Grasserbauer, I. Weissensteiner, G. Falkinger, S. Mitsche, P. J. Uggowitzer, S. Pogatscher, Evolution of Microstructure and Texture in Laboratory- and Industrial-Scaled Production of Automotive Al-Sheets, *Materials*, 13 (2020) 469, doi:10.3390/ma13020469
- ¹⁸ X. Zhao, T. Jin, L. Ding, B. Wan, X. Lei, C. Xu, C. Zhang, Z. Jia, Q. Liu, The effect of combined cold rolling and homogenization on the microstructures and mechanical properties of twin-roll casted 8021

- aluminum alloy, *J. Alloy & Comp.*, 937 (2023) 168385, doi:10.1016/j.jallcom.2022.168385
- ¹⁹ J. Hu, K. Ikeda, T. Murakami, Effect of texture components on plastic anisotropy and formability of aluminium alloy sheets, *J. Mater. Process. Tech.*, 73 (1998) 49–56, doi:10.1016/S0924-0136(97)00211-2
- ²⁰ E. Cantergiani, G. Falkinger, S. Mitsche, M. Theissing, S. Klitschke, F. Roters, Influence of Strain Rate Sensitivity on Cube Texture Evolution in Aluminium Alloys, *Metal. & Mater. Trans. A*, 53A (2022) 2832–2860, doi:10.1007/s11661-022-06710-5
- ²¹ J. Hirsch, Texture and anisotropy in industrial applications of aluminium alloys, *Arch. Metal. & Mater.*, 50 (2005) 21–34
- ²² B. D. Soh Fotsing, M. Fogue, A. Fomethe, G. F. Anago, E. Nguena, Y. Njimkouo, An industrial Method for Reducing the Anisotropy Index of Aluminium 1200 Rolled sheets, *Int. J. Eng. & Tech.*, 2 (2010) 365–372